Microfluidic conformal coating of non-spherical magnetic particles

Byeong-Ui Moon,[1] Navid Hakimi,[2] Dae Kun Hwang,[2] and Scott S. H. Tsai[1,a)]
[1]*Department of Mechanical and Industrial Engineering, Ryerson University, 350 Victoria St., Toronto, Ontario M5B 2K3, Canada*
[2]*Department of Chemical Engineering, Ryerson University, 350 Victoria St., Toronto, Ontario M5B 2K3, Canada*

(Received 7 May 2014; accepted 28 July 2014; published online 6 August 2014)

We present the conformal coating of non-spherical magnetic particles in a co-laminar flow microfluidic system. Whereas in the previous reports spherical particles had been coated with thin films that formed spheres around the particles; in this article, we show the coating of non-spherical particles with coating layers that are approximately uniform in thickness. The novelty of our work is that while liquid-liquid interfacial tension tends to minimize the surface area of interfaces—for example, to form spherical droplets that encapsulate spherical particles—in our experiments, the thin film that coats non-spherical particles has a non-minimal interfacial area. We first make bullet-shaped magnetic microparticles using a stop-flow lithography method that was previously demonstrated. We then suspend the bullet-shaped microparticles in an aqueous solution and flow the particle suspension with a co-flow of a non-aqueous mixture. A magnetic field gradient from a permanent magnet pulls the microparticles in the transverse direction to the fluid flow, until the particles reach the interface between the immiscible fluids. We observe that upon crossing the oil-water interface, the microparticles become coated by a thin film of the aqueous fluid. When we increase the two-fluid interfacial tension by reducing surfactant concentration, we observe that the particles become trapped at the interface, and we use this observation to extract an approximate magnetic susceptibility of the manufactured non-spherical microparticles. Finally, using fluorescence imaging, we confirm the uniformity of the thin film coating along the entire curved surface of the bullet-shaped particles. To the best of our knowledge, this is the first demonstration of conformal coating of non-spherical particles using microfluidics. [http://dx.doi.org/10.1063/1.4892542]

I. INTRODUCTION

Coating of microparticles is a useful approach for applications in drug delivery and cell-based therapies such as cell transplantation therapy.[1–4] For example, in islet transplantation for the treatment of type 1 diabetes, a properly engineered coating layer may protect transplanted cells against host-immune system rejection, while avoiding the chronic use of immunosuppression regimens.[5] This biocompatible coating layer may protect against the immune response by blocking immune cells and antibodies, while the semi-permeable nature of the coating membrane allows small molecules like oxygen and insulin to diffuse in and out.[6]

Cell coating often involves using microencapulsation methods that trap cells inside droplets.[7–9] However, in microencapsulation, the cells are surrounded by a membrane that is typically more than $O(100)$ μm in thickness. The large thickness of the membrane results in long chemical diffusion times that may adversely affect cell survival and function[10] and prevent rapid response of the cells to physiological stimuli.[11]

[a)]Author to whom correspondence should be addressed. Electronic mail: scott.tsai@ryerson.ca

Another particle coating geometry—so-called conformal coating—involves depositing a much thinner layer of a protective membrane on microparticles or cell aggregates.[12] Here, the coating membrane conforms to the shape of the aggregate and minimizes the membrane's contribution to the total transplant volume. This coating geometry reduces molecular transport times through the membrane, and the homogeneous thickness of the coating layer permits uniform transport of molecules to the particle surface.[10]

Conformal coating has been reported using several two-phase flow techniques, namely, selective withdrawal,[13,14] centrifugation,[15] and bulk emulsification.[16] In addition to these hydrodynamics-based methods, other conformal coating techniques that involve surface chemistry include interfacial polymerization,[17] surface binding with polymer-lipid,[18,19] and layer-by-layer poly(L-lysine)(PLL)-PEG copolymer assembly.[20] Magnetic conformal coating by Khademhosseini *et al.*[3] uses a magnetic force to pull cell aggregates that have a magnetic core through polymer layers in a syringe tube. With this magnetic method, the authors are able to conformally coat agarose-immobolized cell aggregates with a coating layer thickness of less than 70 μm.

Magnetic forcing also appears in microfluidics, where it is used to manipulate particles and cells,[21–23] for applications such as trapping,[24] separation[25,26] and sorting.[27] Tsai *et al.*[28] has showed coating of spherical magnetic particles in microfluidics, with magnetic forces applied to move the microparticles from the aqueous to the non-aqueous phase in a co-laminar flow geometry. Upon passage through the co-laminar interface, the microparticles are coated with a thin $O(1)$ μm layer of the aqueous fluid. Since this first demonstration, Tarn *et al.*[29] has developed a similar microfluidic geometry for the washing and binding of a polymer onto magnetically functionalized cells with polyelectrolytes, via passage through multiple co-laminar flows by magnetic forcing in a microfluidic channel. Sinha *et al.*[30] also reported particle dynamics at the interface of a microfluidic co-laminar flow of an aqueous two-phase system (ATPS).

In this paper, we describe the conformal coating of non-spherical magnetic particles using microfluidics. The non-spherical conformal coating geometry we achieve is distinguished from the previous works of coating spherical particles, where the coating layer is naturally a spherical shell around the particle because interfacial tension tries to minimize the encapsulating fluid's surface area. In our experiments, the interaction between the particle surface and the coating layer overcomes the tendency of interfacial tension to form a spherical shell. As a result, the coating layer conforms to the curved surfaces of the non-spherical particles. To the best of our knowledge, this paper is the first to demonstrate the use of microfluidics to perform conformal coating on non-spherical microparticles.

We first describe the manufacture of bullet-shaped magnetic microparticles using stop-flow lithography.[31,32] For coating experiments, we use a modified version of the microfluidic magnetic conformal coating geometry of Tsai *et al.*[28] that controls the spatial position of the particles passing through the co-flow interface. Then, we compare the dynamics of the microparticle coating process as we vary the surfactant concentration in our fluid mixture. We use this information to extract the approximate magnetic susceptibility of our synthesized non-spherical particles. Finally, we use fluorescence imaging to demonstrate the uniform nature of the coating layer on the surface of our bullet-shaped particles.

II. EXPERIMENTAL METHODS

A. Preparation of non-spherical magnetic particles

We synthesized non-spherical magnetic particles using microfluidic stop-flow lithography.[32] UV-induced photopolymerization was performed with a precursor solution introduced into a microfluidic channel (Fig. 1(a)). This precursor solution was prepared by a mixture of 35% (v/v) poly(ethylene glycol) diacrylate (PEG-DA Mw 700, Sigma-Aldrich, St. Louis, MO, USA), 5% (v/v) 2-hydroxy-2-methylpropiophenon (Darcour 1173, Sigma-Aldrich, St. Louis, MO, USA) initiator, 20% (v/v) water-based ferrofluid (EMG 508, Ferrotec, Bedford, NH, USA), and 40% (v/v) deionized (DI) water.

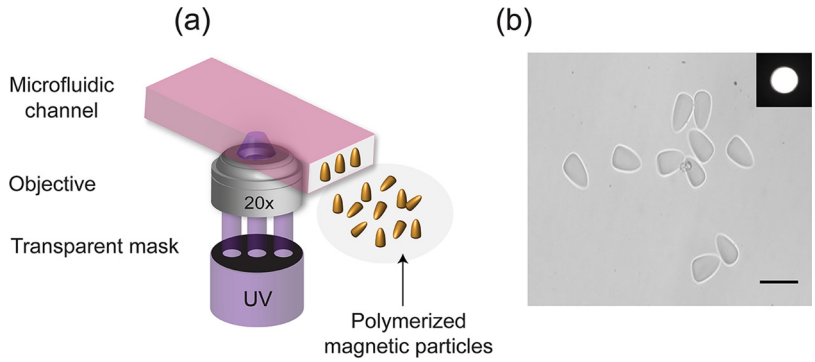

FIG. 1. (a) Schematic diagram of non-spherical magnetic particle synthesis. The microparticles are synthesized using a stop-flow lithography method.[32] UV-initiated photopolymerization in the presence of a magnetic precursor solution produces the non-spherical magnetic particles. (b) An image of the prepared non-spherical magnetic particles. Bullet-shaped magnetic particles are produced with a circle mask design (shown in the inset). Scale bar 50 μm.

An air controlled feeding system was used to introduce the precursor solution into the channel. In-line setup of a pressure regulator valve (Type 100LR, Control Air, Inc., Amherst, NH, USA) and a three-way solenoid valve (Burkert, Germany) controlled the compressed air with repeated on-off cycles. A metal arc lamp (Lumen 200, Prior Scientific, Inc., Cambridge, UK) served as the UV light source, and a digital UV shutter (Lambda SC, Sutter Instruments, Novato, CA, USA) regulated the UV exposure time. The valve and the shutter were both controlled by a customized LabView (National Instruments, Austin, Texas, USA) program.

An inverted microscope (Axio Observer.A1, Zeiss, Oberkochen, Germany) equipped with a 20× objective (20x/0.4 Korr LD Plan-Neofluar, Zeiss, Oberkochen, Germany) was used to produce a cylindrical UV light path through the thickness of the microchannel, and a patterned photomask was placed at the field-stop of the microscope to change the shape of the incident UV light. A UV filter set (11000v2, Chroma Corp., Bellows Falls, VT, USA) was used to screen UV light for the desired UV excitation wavelength.

We produced bullet-shaped magnetic particles using a circle pattern photomask (see, for example, Fig. 1(b)). The water-based ferrofluid added to the prepolymer mixture reduced the opacity of the solution and decreased the UV absorptivity of the solution along the microchannel height. The interference of the UV light caused by the opacity of the solution created a gradient of UV light intensity along the UV light path. This UV light gradient produced bullet-shaped particles with curved surfaces. A diffuse layer of oxygen near the gas-permeable PDMS walls inhibited prepolymer polymerization at the walls. The resulting lubrication layer between particles and the walls permitted removal of the particles by an applied fluid flow.

For continuous mass production, we used a LabView program to tune the UV exposure time and the inlet pressure cycle time in the range of 400–600 ms and 50–200 ms, respectively. This process achieved a particle production rate of 16 particles per second. We prepared approximately 100 000 particles for each batch and stored the particles in a 2 ml Eppendorf tube. The bullet-shaped particles we synthesized have approximate diameters and lengths, 20 and 35 μm, respectively. These particles also have hydrophilic surfaces, which enables their suspension in DI water. The microparticle magnetic susceptibility χ was not known *a priori*; however, we were able to estimate the value of the magnetic susceptibility χ using the method described in Sec. III B.

B. Microfluidic particle coating experiments

Our particle coating microfluidic device was modified from the first generation system reported elsewhere.[28] Fig. 2 shows a schematic diagram of the microchannel design of our particle coating device. Aqueous solution flowed through the buffer inlet, and non-spherical particles suspended in an aqueous phase entered through the particle inlet (Fig. 2(a)). Non-aqueous fluid entered through the oil inlet. At the T-junction (Fig. 2(b)) where particles are introduced

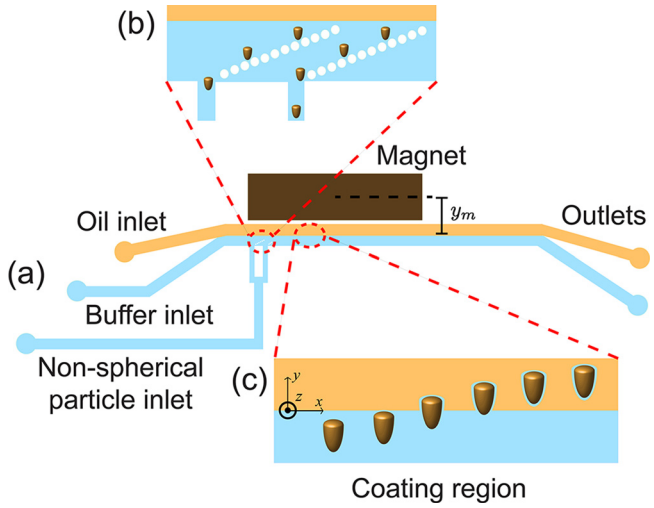

FIG. 2. Schematic diagram of the microfluidic device for conformal coating of non-spherical magnetic particles. (a) The device consists of three inlets where the oil, buffer solution, and non-spherical particle suspension are introduced. A permanent magnet is positioned adjacent to the main co-laminar flow microfluidic channel. Fluid flow is from left to right. (b) An enlarged view of the T-junction where the embedded micropillars guide the magnetic particles to the coating region at the co-flow interface. (c) An enlarged view of the coating region. Here, the non-spherical particles in the aqueous phase pass into the non-aqueous phase and become coated by a thin film of the aqueous phase fluid.

into the co-laminar flow, a pillar array[33] was built into the device to guide all of the particles to a specific coating region in the microchannel (Fig. 2(c)).

The gap between the pillars was 10 μm, and each row of pillars was offset by an angle of 20° from the microfluidic flow direction. A filtering array of pillars (not shown) was used in the particle inlet to prevent debris from clogging the channel. The width and height of the co-flowing channel were 500 and 55 μm, respectively.

Patterning the top polydimethylsiloxane (PDMS, Sylgard 184, Dow Corning, Midland, MI, USA) layer of the device was accomplished using the standard soft lithography technique.[34] Specifically, we used a 10:1 PDMS prepolymer to curing agent ratio in our mixture. A biopsy punch (Integra Miltex, Inc., Rietheim-Weilheim, Germany) was used to create inlet and outlet holes in the PDMS layer. The PDMS and cover glass slide (24 mm × 60 mm, VWR, Radnor, PA, USA) were cleaned with sonication in ethanol and dried with nitrogen gas. After oxygen plasma treatment (Harrick Plasma, Ithaca, NY, USA), the PDMS layer and glass slide were irreversibly bonded.

A 3 mm thick PDMS dummy layer was physically bonded to the bottom of the glass slide, to elevate the microfluidic device vertically. Elevation allowed the microchannel to be positioned along the central axis of the adjacent magnet, so that the vertical component of the magnetic field gradient was eliminated. The PDMS-glass-PDMS assembly was placed on top of another glass slide that was offset by 5 mm so that a magnet stack could be placed on the bottom glass slide.

The three-layer stack of neodymium iron boron (NdFeB) magnets (K. J. Magnetics, Jamison, PA, USA), each with dimensions $\ell_m \times w_m \times h_m = 12.70 \times 6.35 \times 3.18$ mm and magnetization $M = 1.2$ MA m^{-1}, was positioned adjacent to the oil-side of the microchannel. The magnet-center was placed at a perpendicular distance $y_m \approx 6$ mm away from the x-axis of the microchannel (Fig. 2).

Aqueous and non-aqueous solutions were introduced to the microfluidic chip by interfacing with Tygon tubing (Saint-Gobian, La Défense, Courbevoie, France). The non-aqueous solution was dodecane with 10 wt. % Span 80, and the aqueous buffer solution was DI water with 8 mM sodium dodecyl sulfate (SDS). Non-spherical particles were suspended in the same aqueous solution. In some experiments, we reduced the aqueous solution SDS concentration to 2 and 3 mM, to increase the oil-water interfacial tension. This mixture of water and dodecane with

SDS and Span 80 surfactants, respectively, gives an ultralow interfacial tension $\gamma = O(10^{-6}–10^{-5})$ N m^{-1}.[35,36] The viscosities of the aqueous and non-aqueous fluids are $\mu_w = 1$ and $\mu_o = 1.3$ mPa s, respectively.

The non-aqueous fluid was introduced via a syringe pump at a flow rate of 3 μl min^{-1} (Harvard Apparatus, Holliston, MA, USA), and the buffer solution was pumped at a flow rate of 0.5 μl min^{-1}. The particle suspension was supplied by an inlet pressure less than 1 psi. A 200 μl pipette tip was vertically inserted into the particle inlet, and pressurized by compressed air.

Experimental images of particle coating were captured by an inverted microscope (IX71, Olympus Corp., Tokyo, Japan) with 20× or 50× objectives, and an attached high speed camera (Miro M110, Vision Research, Wayne, NJ, USA). The high speed camera operated at a frame rate of 1000 fps and an exposure time of 300 μs. Post-processing of images and particle coating thickness measurements were completed using ImageJ software.

III. RESULTS AND DISCUSSIONS

A. Bullet-shaped microparticles crossing the co-laminar interface

As bullet-shaped particles arrive at the T-junction in the microchannel, the embedded micropillar array (Fig. 2(b)) guides the particles toward the particle coating region (Fig. 2(c)). Here, the particles experience two competing forces: viscous stresses from the co-flowing aqueous fluid push the particles in the axial direction of the channel, and magnetic forces from the field gradient generated by the permanent magnet pulls the particles towards the magnet-side of the channel (see Fig. 2(c)). The embedded micropillars help to guide all of the particles to approach the co-flowing oil-water interface at approximately the same location.

Fig. 3 shows time-series images of two bullet-shaped magnetic particles during the coating process. Here, the images are captured at 4 (Fig. 3(a)) and 20 ms (Fig. 3(b)) time intervals. The aqueous (bottom) and non-aqueous (top) phase fluids are moving from left to right. Bullet-shaped particles approach the co-flowing interface (Fig. 3(a)), deforms the interface, and subsequently passes through the interface (Fig. 3(b)), while being transported downstream by the co-laminar flow.

Upon passage through the moving interface, the microparticles are covered by a thin film of the aqueous phase as they continue to move through the oil phase. As the particles move

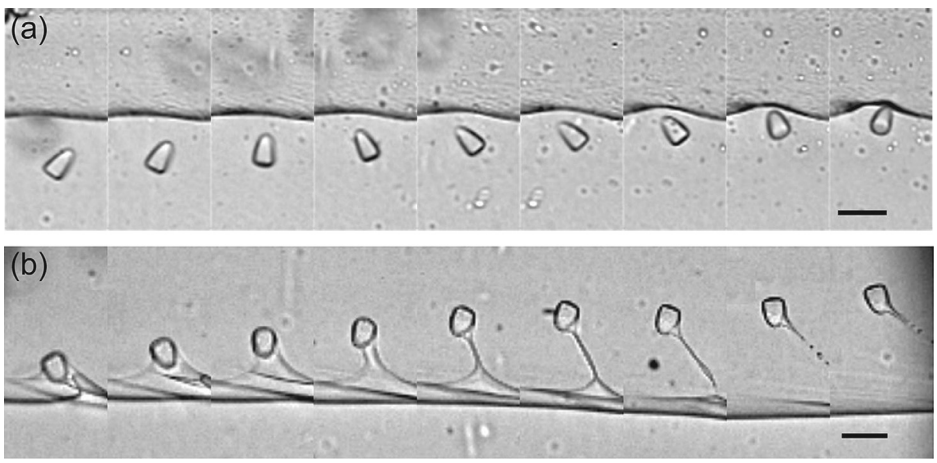

FIG. 3. Time-series experimental images of two particles during the coating process. (a) A bullet-shaped particle approaching the co-laminar interface with its high curvature face pointing towards the interface. (b) Another particle passing through the co-laminar microfluidic interface with its low curvature face pointing towards the interface. Particle orientations appear to continually vary during the coating process. The bullet-shaped magnetic particles move through the aqueous phase (bottom) into the non-aqueous phase (top). The aqueous and non-aqueous fluids flow from left to right at the same speed. As the particles pass through the two-fluid interface, they first deform and then penetrate through the interface. Here, the images are captured in (a) 4 and (b) 20 ms time intervals. Scale bars 50 μm.

farther away from the interface, a comet-like tail of the thin film coating layer forms behind each particle. The tail breaks up into small droplets by a Rayleigh-Plateau type instability (see, for example, the last two frames in Fig. 3(b)).

In low oil-water interfacial tension experiments where the SDS concentrations are 3 or 8 mM in water, we do not observe any noticeable orientation preference of the particles as they are passing through the two-fluid interface. As shown in Figs. 3(a) and 3(b), the particles appear to arrive at the interface at varying orientations (for example, with the high curvature end of the particle facing toward, against, or parallel to the co-flow interface). Particle rotations (Fig. 3(a)) during the coating process may be a result of the interplay between hydrodynamic drag acting on the particle and oil-water interfacial tension acting to resist interfacial deformation by the particle.

B. Estimating microparticle magnetic susceptibility

Fig. 4 shows the x (Fig. 4(a)) and y (Fig. 4(b)) positions of bullet-shaped magnetic particles plotted against time, during the particle coating process. Here, we conduct three experiments using different aqueous solution SDS surfactant concentrations: 2, 3, and 8 mM. Quantifying such ultralow interfacial tensions is challenging, but based on a previous report[36] that uses the same water-dodecane mixture with SDS and Span 80 surfactants, we estimate that our mixtures have approximate interfacial tensions ranging from $O(10^{-6})$ (with 8 mM SDS in water) to $O(10^{-5})$ (with 2 mM SDS in water).

In the flow (x) direction, we do not observe any dependence of the particle speed on the two-fluid interfacial tension (Fig. 4(a)); all of the particles move at approximately the same speed irrespective of the aqueous phase SDS concentration. However, in the transverse (y) direction to the flow, we find dramatic differences in the particle speed. Namely, the rate of penetration of the particles through the oil-water interface grows with increasing aqueous phase SDS concentration. Presumably, increasing the SDS concentration translates into lowering the interfacial tension. Thus, when the interfacial tension is decreased, the particles deform and subsequently cross the interface more rapidly.

In particular, when the aqueous phase SDS concentration is 2 mM (blue diamonds in Fig. 4(b)), we note that the bullet-shaped particles do not deform the oil-water interface sufficiently to pass through the interface. We also notice that most of the microparticles trapped at

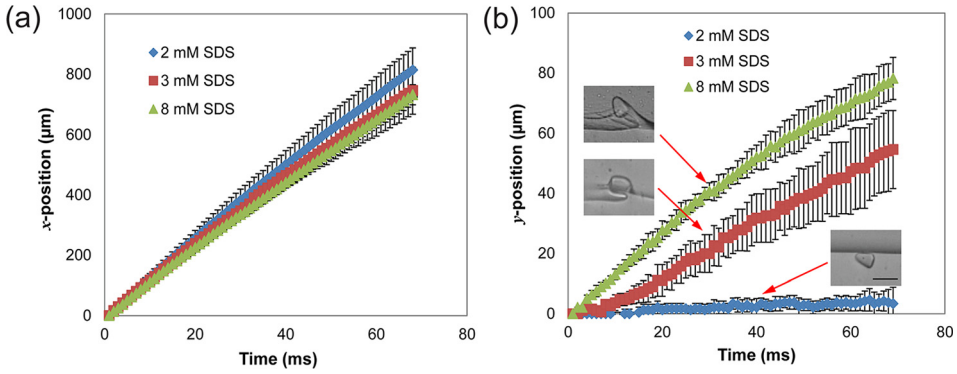

FIG. 4. Plots of the x and y components of particle displacement versus time during the coating process. Here, time $t = 0$ describes the moment when a particle arrives at the oil-water co-flow interface. The aqueous phase SDS concentrations are 2, 3, and 8 mM. (a) In the flow (x) direction, we find that all of the particles are carried by the flow. The particles move at approximately the same speed even as they approach and deform the co-flow interface. (b) Plots of microparticle positions in the transverse (y) direction to the flow, versus time. Here, the aqueous phase SDS concentration influences particle trajectory towards the permanent magnet. At higher SDS concentration, the two-phase interfacial tension is lower. Thus, the particles are able to deform the interface more rapidly (see, for example, the data for 8 mM versus 3 mM SDS). At 2 mM SDS concentration in the aqueous phase, the microparticles are trapped, and do not penetrate the two-phase interface. We exploit the transition between particle passage and trapping to estimate the bullet-shaped particle magnetic susceptibility. Microparticles in the inset images are shown at the time points indicated by the red arrows. We note that for 2 mM SDS in the aqueous phase, the bullet-shaped microparticle is unable to significantly deform the two-phase interface. Error bars indicate one standard deviation. Scale bar 50 μm.

the two-fluid interface are oriented with their long axis parallel to the fluid-fluid interface (see, for example, the right inset image of Fig. 4(b)). Although we have not attempted any energetic modeling of this phenomenon, we anticipate that this particle orientation at the liquid-liquid interface corresponds to the lowest energy orientation state when the interface does not deform significantly. This behavior is in contrast to the interfacial deformation observed when the SDS concentration is 3 and 8 mM (see the two inset images on the left in Fig. 4(b)).

We exploit this transition between particles passing through the interface (3 and 8 mM SDS) and becoming trapped at the interface (2 mM SDS) to deduce the approximate magnetic susceptibility of our synthesized bullet-shaped particles. In the transverse direction to the flow, whether a particle passes through the oil-water interface or remains trapped at the interface depends primarily on a competition between the magnetic force and the force due to interfacial tension (Fig. 5). Thus, in equilibrium, we write the y-direction force balance $F_m - F_\gamma = 0$. Here, the magnetic force

$$F_m = 4\pi a^3 \mu_o \frac{\chi}{\chi + 3} \frac{\partial H^2}{\partial y}, \tag{1}$$

where the particle characteristic length is a (Fig. 5), permeability of free space $\mu_o = 1.257 \times 10^{-6}$ m kg s^{-2} A^{-2}, and the magnetic field is $\boldsymbol{H}$. We assume that the particles are perfectly wetting in the aqueous phase, such that a contact line is absent from the particle surface. Thus, the restoring force due to interfacial tension,

$$F_\gamma = 2\pi\gamma a \sin\theta, \tag{2}$$

where θ is the interfacial deformation defined by the tangent to the interface inflection point (see Fig. 5). We also make the assumption that the transition between particle passage and trapping is dependent on the force balance corresponding to the maximum interfacial restoring force, $F_\gamma \approx 2\pi\gamma a$, where $\sin\theta = 1$.

Recognizing that typically microparticle magnetic susceptibilities $\chi \ll 1$, so that $\frac{\chi}{\chi+3} \rightarrow O(\chi)$, we non-dimensionalize by $\hat{\boldsymbol{H}} = \boldsymbol{H}/M$ and $\hat{y} = y/y_m$, and isolate for the gradient of the squared magnetic field, to find

$$\frac{\partial \hat{H}^2}{\partial \hat{y}} \approx \frac{1}{\varepsilon B}, \tag{3}$$

where the small aspect ratio $\varepsilon = a/y_m$, and the dimensionless magnetic Bond number $\beta = 2\mu_o \chi a M^2/\gamma$.

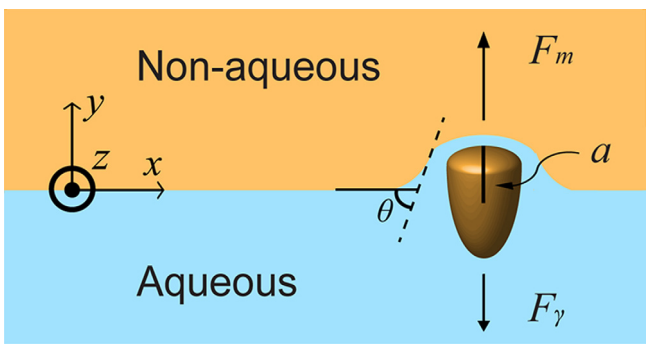

FIG. 5. Schematic diagram of a bullet-shaped particle deforming the interface between the aqueous and non-aqueous fluids in our microfluidic system. Here, we assume that the particle is moving with the fluids from left to right. Therefore, we only consider a force balance in the transverse (y) direction to determine whether or not the particle will cross the interface. The magnetic force F_m exerted on the particle by the applied magnetic field gradient is countered by the force due to interfacial tension F_γ. We extract the magnetic susceptibility of the particle by observing the trapping or passage of the particle at the interface as we vary the SDS concentration in the aqueous phase to change the interfacial tension γ.

At the critical point between particle passage and trapping at the interface, $\partial \hat{H}^2/\partial \hat{y} \approx 1/\varepsilon B = O(1)$. Thus, isolating for the magnetic susceptibility χ and substituting the parameters used in our experiments, we find that our synthesized bullet-shaped microparticles have magnetic susceptibility $\chi = O(10^{-4})$. This value of magnetic susceptibility χ is one order of magnitude less than for commercially available magnetic microspheres.[36] The lower value of the magnetic susceptibility χ in our bullet-shape particles likely results from the lower concentration of iron oxide nanoparticles suspended in our pre-polymer mixture.

C. Fluorescence imaging of particle conformal coating

Figs. 6(a)–6(c) show a time-series of close-up images, extracted from a high-speed video, of the coating of a bullet-shaped particle in our microfluidic device. Here, the particle arrives at the co-laminar flow interface, deforms the interface and eventually breaks away from the interface while dragging some of the lower aqueous phase into the non-aqueous phase (see movie 1 in the supplementary material[37]).

We find that capturing the entire coating process in a single microscope frame is very difficult, because the coating dynamics often occurs through the entire length of the microscope frame. Therefore, we employ fluorescence imaging, downstream of the particle coating region, to image the coating layer.

Fig. 6(d) shows a conformally coated bullet-shaped magnetic particle with fluorescent dye in the coating fluid. In this image, the aqueous solution contains 10 mM fluorescein and 8 mM SDS. For better image recording, we turn on the bright-field light with a minimal intensity to visualize the coating of the non-spherical particles. Movie 2 in the supplementary material[37] shows a video of this fluorescence imaging experiment.

The image (Fig. 6(d)) shows the coating fluid surrounding the bullet-shaped particle in an approximately uniform fashion. We note that the coating layer captures the 3D curvature of the particle, and the coating layer thickness is approximately $1.6 \pm 0.5\,\mu$m along the entire particle surface.

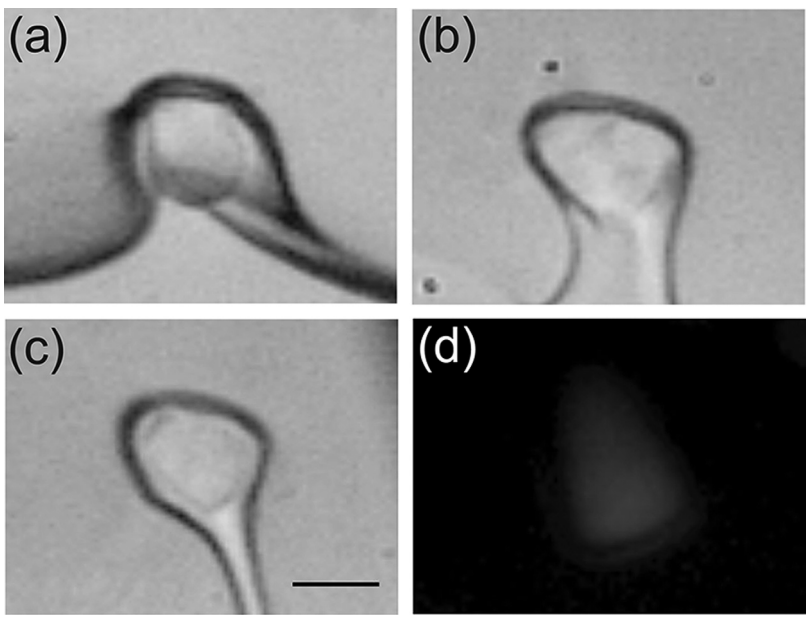

FIG. 6. Close-up views of the coating of a single non-spherical magnetic particle. As the magnetic particle approaches the oil-water interface, it (a) deforms and (b) passes from the aqueous (lower) phase to the non-aqueous (upper) phase. Subsequently, the particle is (c) conformally coated with the aqueous phase, and a tail of the aqueous phase forms behind the particle. This tail eventually breaks up via a capillary instability process. (d) A conformally coated bullet-shaped magnetic particle shown with fluorescent dye in the coating fluid. In this image, the aqueous solution contains 10 mM fluorescein and 8 mM SDS. The image shows the coating fluid surrounding the bullet-shaped particle in an approximately uniform fashion. Scale bar 20 μm.

D. Physical discussions of conformal coating

This microfluidic conformal coating geometry shows many similarities to the classical fluid mechanics problem of the slow motion of a rigid sphere towards a deformable liquid-liquid interface.[38,39] In the classical problem, the driving force is gravity. Thus, when the sphere approaches the liquid-liquid interface, the competition between gravity and the liquid-liquid interfacial tension regulates the rate of liquid drainage between the sphere and the interface. This competition is described by the gravitational Bond number—the ratio between gravitational force and capillary force acting on the sphere.

At low Bond numbers, capillary forces restrict the deformation of the interface. The liquid between the sphere and the interface completely drains out before the sphere breaks through the interface.[39,40] When the Bond number is much greater than unity, gravitational force on the sphere dominates over the restoring force from interfacial tension. The sphere deforms the interface rapidly. As the sphere penetrates and passes the interface, it entrains a "tail" of the original phase. If the sphere surface is wettable to the entrained phase, then the coating layer stays on the sphere surface.[40]

Analogously, in our microfluidic system, the force on the particle due to magnetism replaces the gravitational force (Fig. 5). Thus, competition between magnetism and interfacial tension results in dynamics that is governed by the dimensionless magnetic Bond number $\beta = 2\mu_o \chi a M^2/\gamma$. With experimental values from our microfluidic setup, we find the magnetic Bond number $\beta = O(10^2 - 10^3)$. These values of the magnetic Bond number β agree with our observations: the non-spherical particles deform the interface quickly, and subsequently entrains a layer of coating fluid upon passage through the interface. The aqueous coating fluid remains on the particles because the particles' surfaces are hydrophilic.

We also note that with microparticles in viscosity-dominated fluid systems (for example, in microfluidics), achieving such high Bond numbers is not practical without using ultralow interfacial tension fluid mixtures (since $\beta \propto a/\gamma$). This assessment is in agreement with the previous literature, which also uses a fluid mixture that has an ultralow interfacial tension.[40] In our experiments, the interfacial tensions are $\sim 1000 - 10\,000$ times smaller than in typical oil-water systems.

Finally, although we have not systematically controlled the magnetic Bond number in our system to tune the coating layer thickness; we anticipate that the film thickness will grow with increasing magnetic Bond number β. As the ratio of magnetism to interfacial tension increases, the particles should migrate through the liquid-liquid interface at a faster rate than the rate of film drainage. Therefore, more of the initial fluid phase should be entrained, resulting in a thicker coating layer. This relationship has been described empirically for classical macroscale sphere coating experiments.[41]

IV. CONCLUSIONS

In this article, we demonstrate the conformal coating of non-spherical magnetic particles in a co-laminar flow microfluidic system. We synthesize the bullet-shaped magnetic particles with 3D curvature using a microfluidic stop-flow lithography technique, and we build our microfluidic device using a multi-layer assembly process to remove vertical gradients of the magnetic field.

In coating experiments, we find that the rate of deformation of the oil-water co-laminar interface varies depending on the aqueous phase SDS concentration. We attribute these differences to changes in the two-phase interfacial tension, and we exploit the changes in the particle behavior at the interface—particles either become trapped at the interface or cross the interface—to extract information on the magnetic susceptibility of the particles. We also observe conformal coating of a bullet-shaped particle with fluorescence imaging, and find that the aqueous coating layer is approximately uniform along the entire curved surface of the bullet-shaped particle.

The microfluidic conformal coating technique we show in this article offers an approach to coat non-spherical particles, and preserve the shape and curvature of the particle surface. To

the best of our knowledge, this is the first demonstration of a microfluidic method to coat non-spherical particles conformally by particle passage through a liquid-liquid interface. In addition to the coating of bullet-shaped microparticles, we also coat other microparticles with highly 3D curvatures (see Fig. S1 in the supplementary material[37]). We anticipate that this technique may be useful for conformally coating small non-spherical objects, such as living cells, in microfluidics. In these biological applications, the non-aqueous phase should be replaced with a biocompatible fluid, such as the fluids used in ATPS.

ACKNOWLEDGMENTS

The authors thank I. M. Griffiths for helpful discussions on surface energies and the definition of the interfacial deformation angle. The authors also thank E. Young for reviewing an early draft of this article. S. S. H. Tsai (Grant No. 435514-2013) and D. K. Hwang (Grant No. 386092-2010) both acknowledge funding support from the Canadian Natural Sciences and Engineering Research Council (NSERC) Discovery grants program. S. S. H. Tsai also acknowledges financial support from a Ryerson University Faculty of Engineering and Architectural Science (FEAS) startup grant.

[1]P. de Vos and P. Marchetti, Trends Mol. Med. **8**, 363 (2002).
[2]P. J. Hung, P. J. Lee, P. Sabounchi, R. Lin, and L. P. Lee, Biotechnol. Bioeng. **89**, 1 (2005).
[3]A. Khademhosseini, M. H. May, and M. V. Sefton, Tissue Eng. **11**, 1797 (2005).
[4]Y. Teramura and H. Iwata, Adv. Drug Deliv. Rev. **62**, 827 (2010).
[5]S. Kizilel, M. Garfinkel, and E. Opara, Diabetes Technol. Ther. **7**, 968 (2005).
[6]P. Soon-Shiong, R. E. Heintz, N. Merideth, Q. X. Yao, Z. Yao, T. Zheng, M. Murphy, M. K. Moloney, M. Schmehl, M. Harris, R. Mendez, and P. A. Sandford, The Lancet **343**, 950 (1994).
[7]F. Lim and A. M. Sun, Science **210**, 908 (1980).
[8]C. A. Crooks, J. A. Douglas, R. L. Broughton, and M. V. Sefton, J. Biomed. Mater. Res. **24**, 1241 (1990).
[9]H. Uludag, P. De Vos, and P. A. Tresco, Adv. Drug Deliv. Rev. **42**, 29 (2000).
[10]J. T. Wilson and E. L. Chaikof, Adv. Drug Deliv. Rev. **60**, 124 (2008).
[11]M.-K. Lee and Y. H. Bae, Adv. Drug Deliv. Rev. **42**, 103 (2000).
[12]M. H. May and M. V. Sefton, Ann. N. Y. Acad. Sci. **875**, 126 (1999).
[13]I. Cohen, H. Li, J. L. Hougland, M. Mrksich, and S. R. Nagel, Science **292**, 265 (2001).
[14]J. L. Wyman, S. Kizilel, R. Skarbek, X. Zhao, M. Connors, W. S. Dillmore, W. L. Murphy, M. Mrksich, S. R. Nagel, and M. R. Garfinkel, Small **3**, 683 (2007).
[15]M. V. Sefton, M. H. May, S. Lahooti, and J. E. Babensee, J. Control. Release **65**, 173 (2000).
[16]A. Leung, Y. Ramaswamy, P. Munro, G. Lawrie, L. Nielsen, and M. Trau, Biotechnol. Bioeng. **92**, 45 (2005).
[17]G. M. Cruise, O. D. Hegre, F. V. Lamberti, S. R. Hager, R. Hill, D. S. Scharp, and J. A. Hubbell, Cell Transplant. **8**, 293 (1999).
[18]S. Miura, Y. Teramura, and H. Iwata, Biomaterials **27**, 5828 (2006).
[19]Y. Teramura, Y. Kaneda, and H. Iwata, Biomaterials **28**, 4818 (2007).
[20]J. T. Wilson, W. Cui, and E. L. Chaikof, Nano Lett. **8**, 1940 (2008).
[21]M. M. Gijs, Microfluid. Nanofluid. **1**, 22 (2004).
[22]N. Pamme, Lab Chip **6**, 24 (2006).
[23]M. Tarn, M. Lopez-Martinez, and N. Pamme, Anal. Bioanal. Chem. **406**, 139 (2013).
[24]A. Winkleman, K. L. Gudiksen, D. Ryan, G. M. Whitesides, D. Greenfield, and M. Prentiss, Appl. Phys. Lett. **85**, 2411 (2004).
[25]N. Chronis, W. Lam, and L. Lee, in *Micro Total Analysis Systems*: *Proceedings of the μTAS 2001 Symposium, held in Monterey, CA, USA, 21–25 October, 2001* (Kluwer, Academic Publishers, 2001), p. 497.
[26]N. Pamme and A. Manz, Anal. Chem. **76**, 7250 (2004).
[27]N. Pamme and C. Wilhelm, Lab Chip **6**, 974 (2006).
[28]S. S. H. Tsai, J. S. Wexler, J. Wan, and H. A. Stone, Appl. Phys. Lett. **99**, 153509 (2011).
[29]M. D. Tarn, R. F. Fakhrullin, V. N. Paunov, and N. Pamme, Mater. Lett. **95**, 182 (2013).
[30]A. Sinha, A. K. Mollah, S. Hardt, and R. Ganguly, Soft Matter **9**, 5438 (2013).
[31]D. Dendukuri, S. S. Gu, D. C. Pregibon, T. A. Hatton, and P. S. Doyle, Lab Chip **7**, 818 (2007).
[32]N. Hakimi, S. S. H. Tsai, C.-H. Cheng, and D. K. Hwang, Adv. Mater. **26**, 1393 (2013).
[33]C. Kantak, S. Beyer, L. Yobas, T. Bansal, and D. Trau, Lab Chip **11**, 1030 (2011).
[34]J. C. McDonald, D. C. Duffy, J. R. Anderson, D. T. Chiu, H. Wu, O. J. A. Schueller, and G. M. Whitesides, Electrophoresis **21**, 27 (2000).
[35]S. Ho Cheung, A. Sauret, A. Fernandez-Nieves, H. A. Stone, and D. A. Weitz, Phys. Fluids **22**, 082002 (2010).
[36]S. S. H. Tsai, J. S. Wexler, J. Wan, and H. A. Stone, Lab Chip **13**, 119 (2013).
[37]See supplementary material at http://dx.doi.org/10.1063/1.4892542 for experiments with other non-spherical particles and movies of the coating experiments.
[38]S. Hartland, J. Colloid Interface Sci. **26**, 383 (1968).
[39]A. S. Geller, S. H. Lee, and L. G. Leal, J. Fluid Mech. **169**, 27 (1986).
[40]J. W. J. de Folter, V. W. A. de Villeneuve, D. G. A. L. Aarts, and H. N. W. Lekkerkerker, New J. Phys. **12**, 023013 (2010).
[41]O. Pitois, P. Moucheront, and C. Weill, C. R. Acad. Sci. Paris **327**, 605 (1999).